


PDE4 inhibitor eliminates breast cancer stem cells via noncanonical activation of mTOR

Pritha Mukherjee¹ | Arka Bagchi² | Ananya Banerjee¹ | Himansu Roy³ |
Arijit Bhattacharya⁴ | Arunima Biswas² | Urmi Chatterji^{1,5} 

¹Cancer Research Laboratory,
Department of Zoology, University of
Calcutta, Kolkata, India

²Molecular Cell Biology Laboratory,
Department of Zoology, University of
Kalyani, Kalyani, India

³Department of Surgery, Calcutta Medical
College, Kolkata, India

⁴Department of Microbiology, Adamas
University, Kolkata, India

⁵Centre for Research in Nanoscience and
Nanotechnology, University of Calcutta,
Kolkata, India

Correspondence

Urmi Chatterji, Cancer Research
Laboratory, Department of Zoology,
University of Calcutta, 35 Ballygunge
Circular Rd, Kolkata 700019, India.
Email: urmichatterji@gmail.com

Arunima Biswas, Molecular Cell Biology
Laboratory, Department of Zoology,
University of Kalyani, Nadia,
Kalyani 741235, India.
Email: arunima10@gmail.com and
arunima10@klyuniv.ac.in

Funding information

Department of Biotechnology,
Government of West Bengal, India,
Grant/Award Number: 248(Sanc)/BT
(Estt)/RD-27/2016

Abstract

Ineffective cancer treatment is implicated in metastasis, recurrence, resistance to chemotherapy and radiotherapy, and evasion of immune surveillance. All these failures occur due to the persistence of cancer stem cells (CSCs) even after rigorous therapy, thereby rendering them as essential targets for cancer management. Contrary to the quiescent nature of CSCs, a gene profiler array disclosed that phosphatidylinositol-3-kinase (PI3K), which is known to be crucial for cell proliferation, differentiation, and survival, was significantly upregulated in CSCs. Since PI3K is modulated by cyclic adenosine 3',5' monophosphate (cAMP), analyses of cAMP regulation revealed that breast CSCs expressed increased levels of phosphodiesterase 4 (PDE4) in contrast to normal stem cells. In accordance, the effects of rolipram, a PDE4 inhibitor, were evaluated on PI3K regulators and signaling. The efficacy of rolipram was compared with paclitaxel, an anticancer drug that is ineffective in obliterating breast CSCs. Analyses of downstream signaling components revealed a switch between cell survival and death, in response to rolipram, specifically of the CSCs. Rolipram-mediated downregulation of PDE4A levels in breast CSCs led to an increase in cAMP levels and protein kinase A (PKA) expression. Subsequently, PKA-mediated upregulation of phosphatase and tensin homolog antagonized the PI3K/AKT/mTOR pathway and led to cell cycle arrest. Interestingly, direct yet noncanonical activation of mTOR by PKA, circumventing the influence of PI3K and AKT, temporally shifted the fate of CSCs toward apoptosis. Rolipram in combination with paclitaxel indicated synergistic consequences, which effectively obliterated CSCs within a tumor, thereby suggesting combinatorial therapy as a sustainable and effective strategy to abrogate breast CSCs for better patient prognosis.

KEYWORDS

autophagy, cAMP, cancer stem cells, mTOR, PDE, rolipram

1 | INTRODUCTION

Attempts to identify strategies to obliterate cancer stem cells (CSCs) for a more complete remission of tumors have delineated several intracellular molecules, modulation of which led to reduced stemness and metastatic properties and enhanced chemosensitivity of these cells.^{1,2} Interestingly, among different intracellular regulators elucidated by a profiler array were factors related to the phosphatidylinositol-3-kinase (PI3K)/Akt pathway,² which are known to monitor different signaling molecules within the CSCs and help in their maintenance.³ Consequently, upregulation of PI3K (phosphatidylinositol 3' kinase) levels in breast CSCs (brCSCs) compared to normal mammary stem cells prompted investigation of specific molecules related to the PI3K/Akt pathway that were orchestrating events, which led to the perpetuation of stemness and chemoresistance of the CSCs. Although activation of the PI3K/Akt pathway in cancer cells is known to modulate various substrates including mTOR, a master regulator of protein translation,^{3–8} its role in brCSCs is largely unknown. It has however been reported that Akt can directly regulate apoptosis by phosphorylating and inactivating proapoptotic proteins such as BAD, which controls the release of cytochrome *c* from the mitochondria^{9,10}; hence, several preclinical studies and clinical observations have targeted the PI3K/Akt/mTOR pathway as a therapeutic strategy in human cancers.¹¹

Cyclic adenosine 3',5' monophosphate (cAMP) and protein kinase A (PKA) are known to cooperate with PI3K to control the growth and survival of cells.¹² Although cAMP regulates the growth of many cell types,^{13,14} interestingly, it also inhibits proliferation in selected cells;^{15,16} the precise mechanisms by which cAMP differentially inhibits or permits cell cycle entry in CSCs remain undefined.¹⁷ Intracellular levels of cAMP are regulated by disparate activities of two enzymes, adenylate cyclase and phosphodiesterases (PDEs).^{17,18} Extracellular signals activate G-protein-coupled adenylate cyclase, which catalyzes the formation of the cyclic nucleotide (cNT) from its nucleotide triphosphate precursor, and affects the activity of downstream effector molecules including kinases, ion channels, transcription factors, and scaffolding proteins. On the other hand, cNT signals are largely dependent on the expression and activity levels of cNT PDE enzymes, which catalyze the hydrolytic breakdown of cNTs, as from cAMP to 5'-AMP, to terminate its signal.¹⁹ The ATP-binding cassette (ABC) transporters, which are overexpressed in the CSCs, contribute to cAMP compartmentalization across extracellular and intracellular membranes. Two of the members of the ABC transporter family, MRP4/ABCC4

and MRP5/ABCC5, have demonstrated an energy-dependent export of cNTs²⁰ and function as cNT over-flow pumps when there is either an overproduction of cNTs or inhibited PDE activity.^{21,22} Despite relatively equal levels of adenylate cyclase and PDE expression in most cell types, the rate of cAMP hydrolysis in human tissues far exceeds the rate of synthesis, making PDE enzymes important determinants of intracellular cAMP levels, subsequent signaling,²³ and eventually targets for cancer therapy.

Both cAMP and cGMP signaling have been found to have either positive or negative effects on cell growth and survival, depending on cell or tissue type.^{24–26} These observations suggest that aberrant cNT signaling may play an important role in tumorigenesis.^{27,28} The crosstalk between antiproliferative and proapoptotic effects in tumor epithelial cells can therefore be attributed to specific PDE activity. Since alterations in cNT signaling are common to a number of cancer types, these pathways could provide new molecular targets for cancer chemoprevention and chemotherapy. Consequently, we have attempted to delineate the effect of PDEs, specifically in brCSCs, to establish an association between cAMP and cAMP-dependent PKA modulation on the survival of the CSC population. Selectivity and improved toxicity profile achieved by targeting PDEs seem to be promising as an anticancer strategy, especially since PDE inhibitors are already being implemented as drugs. However, the regulatory mechanisms and potential adaptations of CSCs to PDE inhibitors need to be discerned to establish them as putative anticancer drugs for effective chemotherapy and better patient prognosis.

2 | MATERIALS AND METHODS

2.1 | Cell lines and reagents

Human triple-negative breast cancer cell lines MDA-MB-231 and MDA-MB-435s were obtained from National Centre for Cell Sciences, India. Cells were tested for the presence of mycoplasma or other contaminants before proceeding with experiments. Paclitaxel (Pax), rolipram (Rlm), epithelial growth factor, 3-methyladenine (3-MA) and H-89 were from Sigma-Aldrich. Small interfering RNA (siRNA) for PKA was procured from Qiagen. Aldefluor reagent and collagenase-hyaluronidase mix were from Stem Cell Technologies; cAMP ELISA Assay Kit was obtained from Cayman Chemicals; Optiblot ECL Detect Kit and cellular ROS/Superoxide Detection Assay Kit from Abcam; B27 and hydrocortisone were from Life Technologies. Primary and secondary antibodies were from Abcam, Cell Signaling Technology, Sigma-Aldrich, and Santa-Cruz Biotechnology.

2.2 | Drugs

Pax was dissolved in sterile dimethyl sulfoxide (DMSO) at a concentration of 1 mg/ml. Rlm was dissolved in sterile ethanol to make a stock solution of 25 mM. Drugs were diluted from stock solutions into a medium for respective experiments.

2.3 | Cell culture

MDA-MB-231 and MDA-MB-435s were maintained in Dulbecco's modified Eagle's medium (DMEM) supplemented with 10% heat-inactivated fetal bovine serum, penicillin–streptomycin–amphotericin B at 37°C in a humidified 5%–95% air CO₂ atmosphere.² Cells were passaged every 3 days.

2.4 | Culture of mammospheres from cell lines

Cells were plated in ultra-low attachment plates at a density of 2000 cells/ml. Spheres were grown in serum-free DMEM-F12 media supplemented with 0.1 mg/ml B27, 10 ng/ml human epidermal growth factor, 1 mg/ml hydrocortisone, and 10 mg/ml insulin.²

2.5 | Collection and processing of breast tissues

Normal breast tissues and breast tumor tissues were obtained from Medical College and Hospital in Kolkata, in compliance with the Institutional Human Ethical Guidelines and after procuring informed consent from patients. Breast tumors were exclusively primary-site cancers that were either naive or had been subjected to chemotherapy before surgery. Tissues were collected from tumors and nontumor regions (apparently non-affected regions approximately 5–6 in. away from or diagonally opposite to the tumor site) by modified radical mastectomy surgeries or from reduction mammoplasty cases. A total of 50 triple-negative breast cancer (TNBC; ER⁻, PR⁻, HER2/neu⁻) patient samples (stage 2 or stage 3) primarily 25–45 years with no other major infection or diseases have been described. The integrity of the normal and tumor tissues was authenticated by trained professional pathologists. Histologic type of tumors was determined according to World Health Organization classification and graded by the modified Bloom–Richardson grading system.²⁹ Immunohistochemical testing for ER, PR, and HER2/neu was applied to all cases. Tissues

collected were dissociated enzymatically using 1× collagenase–hyaluronidase mix at 37°C for 16–18 h.²

2.6 | In vitro mammosphere culture from human tissues

After enzymatic digestion, primary normal and tumor cells were seeded at 2.5×10^4 cells per well in ultralow attachment plates. Mammospheres were photographed, counted, and sphere formation efficiency was calculated by dividing the total number of spheres formed by the total number of live cells seeded multiplied by hundred.²

2.7 | Cell viability assay

3-(4,4-Dimethylthiazol-2-yl)-2,5 diphenyltetrazolium bromide (MTT) assay has been widely applied in the assessment of cytotoxic drugs.³⁰ A total of 3×10^3 cells/well TNBCs and 2×10^2 MDA-MB-231 cells for mammospheres were seeded in 96-well plates and treated with Rlm at different concentrations (for adherent cells 0–100 mM; for spheroids 0–25 mM) for 24 h. Twenty microliters of MTT solution was added and incubated for 3 h at 37°C. The purple formazan crystals were dissolved in 100 µl DMSO and the absorbance was recorded at 570 nm in a SpectraMax 190 device (Molecular Devices).

2.8 | cAMP assay

Evaluation of cAMP was achieved using a sandwich enzyme-linked immunosorbent assay (ELISA)-based assay, which essentially is dependent on a standard curve construction for cAMP (pmol/ml) following the manufacturer's protocol, and all the experimental values were denoted from the standard curve. The assay sensitivity is around 0.1 pmol/ml. MDA-MB-231 cells were plated at 4×10^5 cells per 6-well plate and grown until 65%–70% confluence. After relevant drug treatments, the cells were washed and treated with 0.1 M HCl for 20 min, and then lysed by sonication. Samples were analyzed for cAMP levels using a direct cyclic AMP Enzyme Immunoassay Kit according to the manufacturer's instructions. Briefly, the assay is based on *para*-nitrophenylphosphate as a substrate and a polyclonal antibody to cAMP to bind in a competitive manner. Reactions were stopped using trisodium phosphate and the color intensity was measured at 405 nm.³¹ Data are expressed as mean values and standard errors of triplicate samples per treatment group.

2.9 | Western blot analysis

Cells/tumors were collected in an ice-cold RIPA buffer. Proteins were resolved by sodium dodecyl sulfate-polyacrylamide gel electrophoresis (SDS-PAGE), transferred onto polyvinylidene fluoride membranes, and probed with the respective primary antibodies (1:1000 dilution) overnight at 4°C. Blots were subsequently incubated with secondary antibodies (1:3000 dilution) for 1 h at room temperature.² For all experiments, β -tubulin was used as the loading control. Luminol was used for immune detection and analyzed using the Gel Doc (Bio-Rad). The band intensities were quantified using Image J software (Bio-Rad Laboratories).

2.10 | Flow cytometric analysis of DNA content of breast cancer cell lines

After treatment with drug and inhibitors, cells were fixed with 70% ethanol for 1 h at 4°C. Next, cells were permeabilized with 0.1% Triton X-100 containing RNaseA (20 μ g/ml). Cells were stained with propidium iodide (PI) and subjected to analysis using BD FACSVerse™ (BD Biosciences). The data were analyzed using the BD FACSuite™ software.^{1,2}

2.11 | Analysis of aldehyde dehydrogenase (ALDH) activity

MDA-MB-231 cells and mammospheres were stained for 45 min at 37°C using ALDEFUOR reagent following the manufacturer's instructions. Cells treated with diethylaminobenzaldehyde, a specific ALDH inhibitor, were used as a control.² The ALDH⁺ population was sorted using a BD FACS Aria™ III with a 488-nm blue laser and a standard fluorescein isothiocyanate (FITC) 530/30-nm band pass filter. Analysis of populations was done using the BD FACSDiva™ Software.

2.12 | Annexin V/PI double staining

A total of 1×10^6 cells were treated with Rlm and Pax for 24 h. MDA-MB-231 mammospheres were treated with Rlm for 12, 24, 48, and 72 h. Apoptosis was determined using annexin V-FITC/PI double staining method.³² Results were obtained on the BD FACSVerse™ (BD Biosciences) and analyzed using the BD FACSuite™ software.

2.13 | Determination of autophagy by flow cytometry

Cells were stained with 1 μ g/ml acridine orange in a complete culture medium for 15 min at room temperature and analyzed on a BD FACSVerse™. Data were analyzed using BD FACSuite™ software. The red-to-green fluorescence ratio was recorded.³³ Autophagy inhibition was achieved by treating cells with 1 mM 3-MA, followed by subsequent drug treatments for 24h.

2.14 | Cellular proliferation assay

A total of 1×10^6 cells were stained with 10 μ l of FITC-conjugated Ki-67. Samples were incubated on ice for 20 min. For DNA staining, 5 μ l of propidium iodide and 70 μ l of RNase (1 mg/ml) were added and samples were incubated at 4°C for 20 min. Cells were immediately assessed by flow cytometry (BD FACSVerse™). Results were analyzed using the BD FACSuite™ software.²

2.15 | RNA-mediated interference by siRNA transfection

RNA interference was performed using HiPerfect Transfection Reagent with specific PKA siRNA. Mammospheres were grown in 6-well low-adherent plates at 2×10^3 cells/well in an antibiotic- and serum-free medium. After 24 h, cells were transfected with 100 pmol of PKA-siRNA or control siRNA/scrambled siRNA (negative control) according to the manufacturer's protocol. Cells were processed after 48 h for subsequent experiments.²

2.16 | Coimmunoprecipitation assay

Mammospheres were harvested in RIPA buffer, to which 5 μ l of anti-Bcl-1 antibody was added and incubated at 4°C for 2 h before the addition of 50 μ l of agarose-protein A/G beads and incubated overnight at 4°C. The immunoprecipitates were resolved by SDS-PAGE and immunoblotted with the Bcl-2 antibody.³⁴ The amount of Bcl-2 that coimmunoprecipitated with Beclin1 was documented. The band intensities were quantified using Image J software. Similarly, for the interaction of mTOR and PKA, cell lysates were immunoprecipitated with phospho-mTOR (pmTOR) and immunoblotted with PKA1 α reg.

2.17 | Homology modeling and protein–protein docking

The homology model structures of mTORC (residues 17–2549) and PKAR1 α (residues 93–378) were built using the protein template structures from the Protein Data Bank (PDB) entries 6BCU and 6NO7. The model structures were built using a fully automated protein structure homology modeling server SWISS-MODEL (<http://swissmodel.expasy.org/>).³⁵ The model quality was estimated based on the QMEAN scoring functions of -2.45 and -0.55 , respectively, which were within the acceptable range.³⁶ Each structure was further validated with Procheck³⁷ with $<1\%$ residues in the disallowed region of Ramachandran plot. PyMOL v1.3 was used to visualize the structural models.³⁸ Protein–protein docking was performed with the two models using high ambiguity-driven protein–protein docking (HADDOCK)³⁹ after defining the restraints using CPORT.⁴⁰ The best-docked structures were selected based on calculations, according to their intermolecular energy, namely, a weighted sum of desolvation, van der Waals, electrostatic interactions, and ambiguous interaction restraints. The interface and stabilization energy of the complex was analyzed by PDBePISA⁴¹ and Prodigy,⁴² respectively.

2.18 | Statistical analysis

All experiments were performed in triplicates. Data are presented as the mean \pm SD of “ n ” independent measurements, as indicated in the figure legends. Statistical comparisons between treated and untreated control groups were calculated by analysis of variance F , followed by Tukey's honestly significant difference. $p \leq 0.05$ was considered significant.

3 | RESULTS

3.1 | Elevated PDE4A expression led to a reduction of cAMP levels in TNBCs and brCSCs

Following results of a differential gene profiler, where upregulation of PI3K was observed in brCSCs in contrast to normal stem cells (NSCs),² a String analysis (node and edge interactions) was carried out to identify different protein–protein associations (Figure 1A). Interactions of PI3K with its positive regulator PKA and negative regulator phosphatase and tensin homolog (PTEN) were evident. In accordance with the predicted interactions,

Figure 1B denotes a schematic representation of the putative signaling pathway, which may regulate the survival of cancer cells. The switch is turned on when cAMP binds to the regulatory subunit of PKA_{inactive} releasing the catalytic subunits of PKA to convert it to PKA_{active}. This in turn stimulates Akt and mTOR to finally suppress autophagy in these cells. However, contrary to our expectations, PKA expression was lower in TNBCs and chemo-treated (CT) breast tumors compared to normal breast tissues, as well as in brCSCs from CT tumor in contrast to NSCs (Figure 1C).

ELISA-based cAMP assays revealed a concomitant reduction in levels of cAMP in tumor tissues compared to adjacent normal counterparts (Figure 1D). Simultaneously, expression of PDE4A1 protein was higher in the TNBC breast tumors (both naive and CT) as compared to their normal counterparts (Figure 1E). cAMP level was also significantly lower in the brCSCs isolated from TNBC tumors compared to NSCs (Figure 1F), concomitant with higher PDE4A1 expression in the CSCs from CT TNBCs (Figure 1G). CSCs of TNBC tumors showed lower levels of cAMP and PKA even after chemotherapy, serving as a major contributor to survivability and stemness properties of CSCs in breast tumors.

3.2 | Rlm reversed cAMP levels and reduced stemness of brCSCs

The effect of different doses of Rlm (0–100 mM) on MDA-MB-231 cells showed a significant dose-dependent reduction in cell viability and defined a half-maximal inhibitory concentration (IC₅₀) value of 1 mM ($p = 0.000191$; Figure 2A). Similar results were seen for MDA-MB-435s cells (Supporting Information: Figure S1A). Rlm significantly decreased PDE4A1 levels in breast cancer cells (Figure 2B). Concomitant increase in cAMP levels from 10.02 pmol/ml in untreated controls to 39.8 pmol/ml at half IC₅₀ (0.5 mM) and 40.5 pmol/ml ($p = 0.000156$) at IC₅₀ (1.0 mM) was observed ($p = 0.000101$; Figure 2C). Comparable results were observed in MDA-MB-435s cells (Supporting Information: Figure S1B). Expression of PDE4A1 was significantly higher in spheroids compared to monolayer cultures (Figure 2D), and the corresponding cAMP levels were reduced in spheres derived from both untreated (UT) tumors (from 12.65 to 9.76 pmol/ml; $p = 0.002607$) or from CT patient samples (from 15.98 to 11.73 pmol/ml; $p = 0.00855$) as compared to two-dimensional (2D) primary cultures from same samples (Figure 2E). The effect of Rlm (0–25 mM) on mammospheres derived from MDA-MB-231 cells showed an IC₅₀ value of 10 mM ($p = 0.0002$) when treated for 24 h

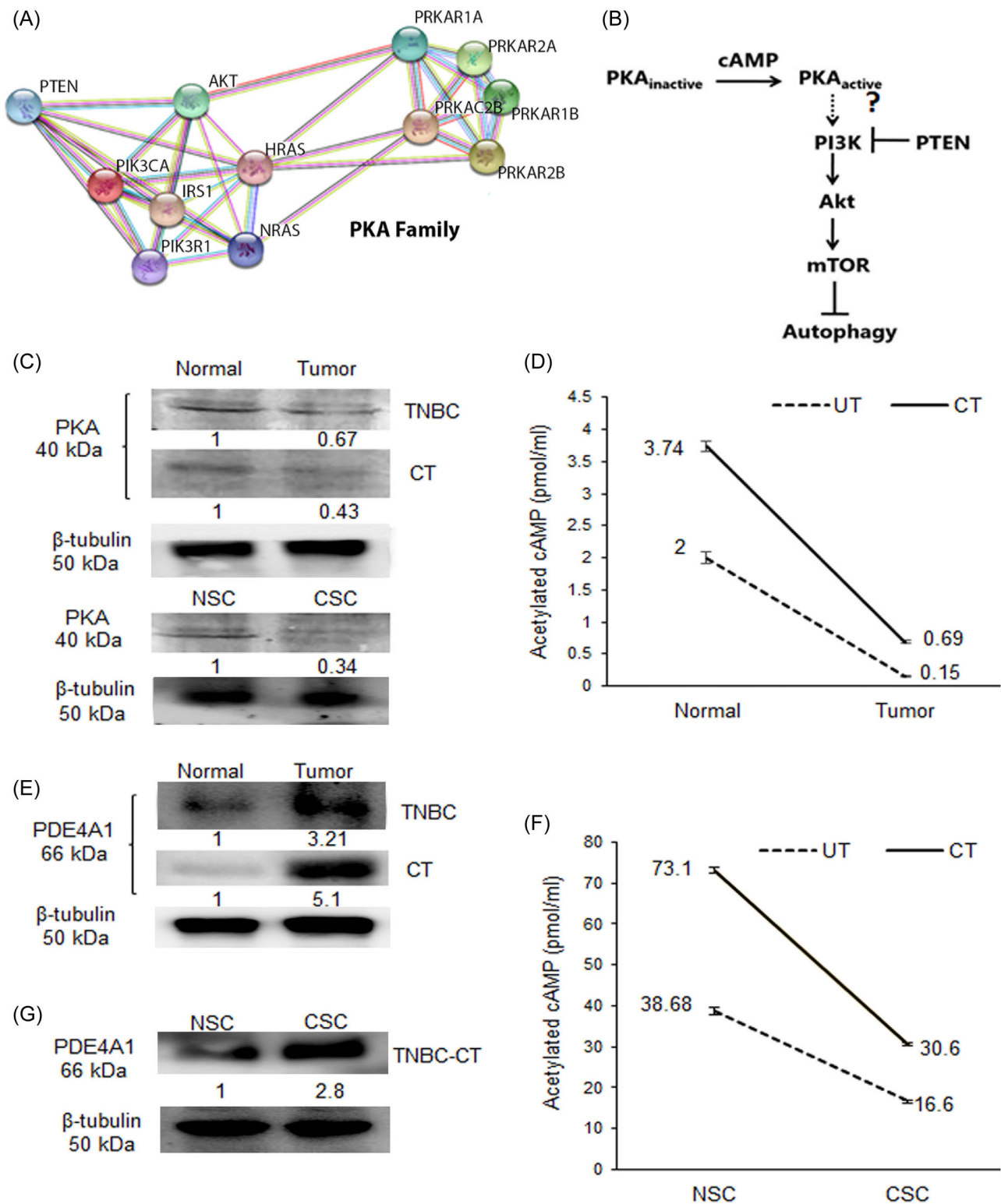


FIGURE 1 Differential levels of cAMP are regulated by PDE4A expression in breast tumors and brCSCs. (A) String analysis showing protein interaction networks between PI3K, PTEN, and PKA. (b) Schematic representation of the signaling cascade and interactions that are presumed to function in breast tumors. (C) Expression of PKA from the normal breast tissue and breast tumors (TNBC, CT) and stem cells (NSC, CSC). (D) Cyclic AMP assay from UT and CT tumor samples compared to adjacent normal mammary tissues. (E) Protein expression of PDE4A1 from naive and CT breast tumors. (F) Cyclic AMP assay from UT and CT CSCs compared to adjacent NSCs. (G) Protein expression of PDE4A1 from CT CSC isolated from TNBC tumor. Comparisons were made with the adjacent normal mammary tissues. Values indicate fold changes in protein expression corresponding to band intensity. Molecular weights are indicated in kilodalton (kDa). Data are representative of three independent experiments. brCSC, breast CSC; cAMP, cyclic adenosine 3',5' monophosphate; CSC, cancer stem cells; CT, chemo-treated tumor; NSC, normal stem cells; PDE4A, phosphodiesterase 4A; PI3K, phosphatidylinositol-3-kinase; PKA, protein kinase A; PTEN, phosphatase and tensin homolog; TNBC, triple-negative breast tumor; UT, untreated.

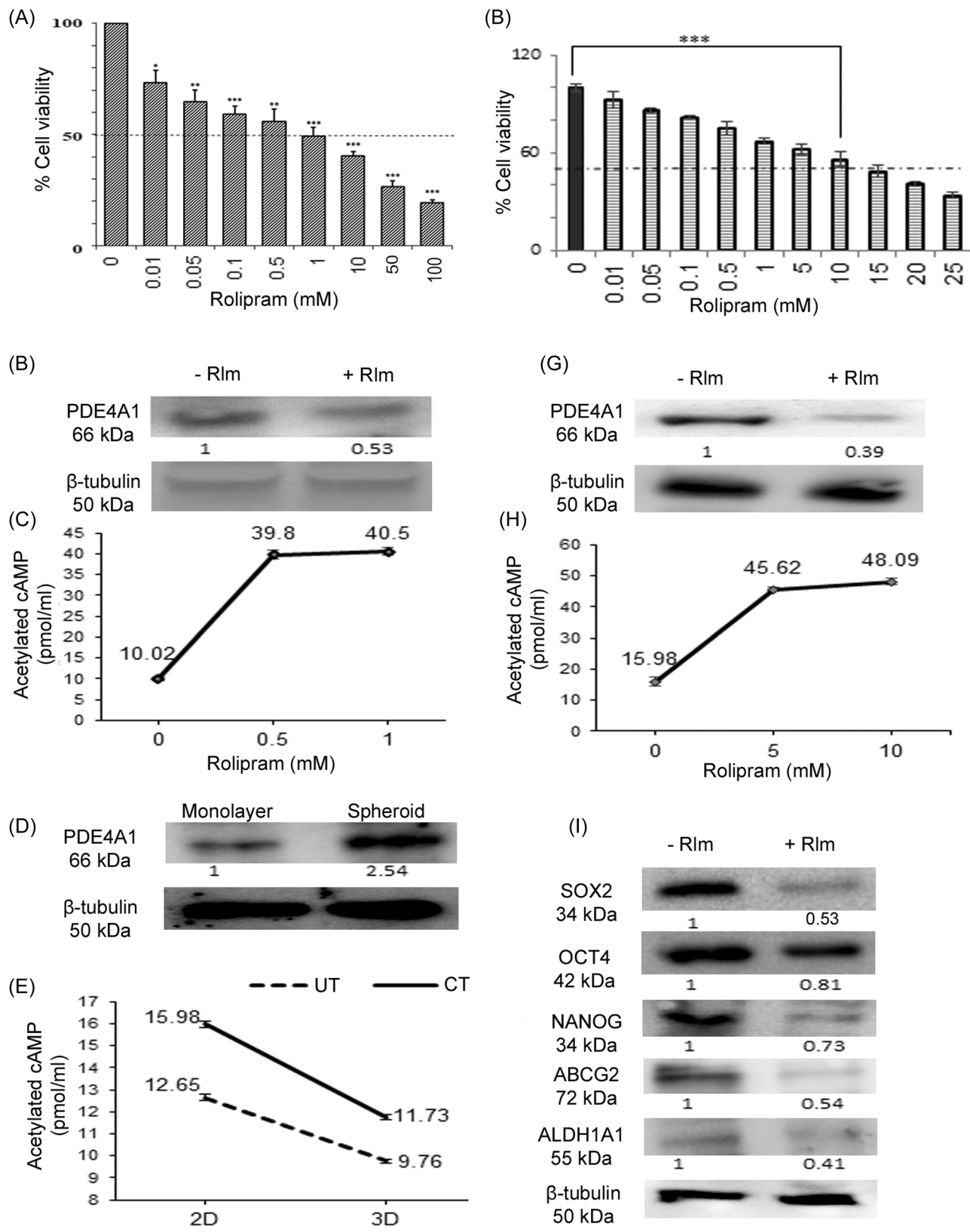


FIGURE 2 (See caption on next page)

(Figure 2F). Rlm significantly reduced PDE4A1 levels in brCSCs as shown by western blot analysis (Figure 2G) and increased cAMP levels to 45.62 pmol/ml ($p = 0.000697$) at half IC_{50} dose (5 mM) and to 48.09 pmol/ml ($p = 0.000695$) at IC_{50} dose (10 mM; Figure 2H). In addition, treatment with Rlm significantly reduced the expression of major stem cell markers (SOX2, OCT4, NANOG, ABCG2, ALDH1A1) in brCSCs (Figure 2I). Rlm treatment induced loss of cell viability by reducing PDE4A1 and increasing cAMP levels in both TNBC cells and mammospheres.

3.3 | Rlm and Pax combination enhanced cytotoxicity and induced autophagy-mediated apoptosis in breast cancer cells

Cellular toxicity and loss of cell viability were observed in MDA-MB-231 cells by trypan blue dye exclusion test (Figure 3A and Supporting Information: Figure S2A) in response to a combinatorial effect of Rlm + Pax treatment (5-fold; $p = 0.000896$) in comparison to Pax individually (3.1-fold; $p = 0.000961$) or Rlm individually (2.8 fold; $p = 0.00718$). Cellular toxicity of MDA-MB-435s cells indicated a similar trend (Supporting Information: Figure S1C). Dual staining with Ki67-FITC and PI indicated significant reduction in proliferating cells by Rlm + Pax (1.6-fold; $p = 0.001273$) in comparison to treatment with Pax (1.2-fold; $p = 0.004961$) and Rlm (1.4-fold; $p = 0.0011$) individually (Figure 3B and Supporting Information: Figure S2B). In contrast to Pax, which led to a G_2/M phase arrest, Rlm induced significant cell cycle arrest of MDA-MB-231 cells at the G_1 phase (2.8-fold; $p = 0.000147$). Interestingly, cotreatment with Pax also indicated a G_1 phase arrest (3.2-fold; $p = 0.000124$) along with increased cells in the sub- G_1 phase (Figure 3C and Supporting Information: Figure S2C). Acridine orange staining revealed that the combination Rlm + Pax induced autophagy in MDA-MB-

231 cells (11.4-fold; $p < 0.001$), in contrast to Rlm (5.61-fold; $p = 0.000188$) and Pax individually (1.9-fold; $p = 0.000414$; Figure 3D and Supporting Information: Figure S2D). Simultaneously, annexin V/PI staining showed that Rlm + Pax induced apoptosis in MDA-MB-231 cells (47.2%), which was almost 10% higher ($p < 0.001$) than treatment with Rlm (37.7%; $p < 0.001$) or Pax (35.5%, $p < 0.001$) individually (Figure 3E and Supporting Information: Figure S2E). Apoptosis was comparable in MDA-MB-435s cells too (Supporting Information: Figure S1D). Additionally, a combination of Rlm + Pax increased cAMP levels ($p = 0.000623$) in MDA-MB-231 cells, as compared to Pax individually, which was almost insignificant compared to control (Figure 3F). Inhibition of cellular proliferation was further ascertained by a significant decrease in the expression of cell cycle regulators (Figure 3G) and increased expression of autophagy and apoptosis regulators (Figure 3G). Increased expression of LC3-II was observed in Rlm-treated cells as well as in Rlm + Pax-treated cells.

From the above findings, it could be summarized that although Pax treatment individually was mostly ineffective, a combination of Rlm + Pax could significantly reduce the expression of PDE4A1 (Figure 3H), along with modulation of the downstream components of the predicted pathway, viz., PKA, PTEN, PI3K, AKT, and mTOR in human TNBC cells. A concomitant increase in cAMP levels led to enhanced expressions of cellular PKA and PTEN (Figure 3H) and reduced expressions of PI3K, AKT, and pmTOR (Figure 3H), thereby corroborating that reduced pmTOR enhanced cellular autophagy, as seen in Figure 3D. The pmTOR and mTOR densitometric ratio was observed to be 1, 0.75, 0.66, and 0.38 in control, Pax-treated, Rlm-treated, and Pax + Rlm-treated cases, respectively (Figure 3H). The combination treatment also showed increased expression of cleaved caspase 3 (cl-caspase 3) in MDA-MB-231 cells (Figure 3H), which confirmed induction of apoptosis, as seen in Figure 3E

FIGURE 2 Rlm reduces the stemness of cancer stem cells by regulating cAMP/PDE4A1 levels. (A) Effect of Rlm on the viability of breast cancer cell MDA-MB-231 determined by the MTT assay after 24 h of treatment. (b) Expression of PDE4A1 in MDA-MB-231 cells in the presence and absence of Rlm (1 mM). (C) cAMP levels of Rlm treated (0.5 and 1 mM) MDA-MB-231 cells as compared to untreated controls. (D) Expression of PDE4A1 protein in MDA-MB-231 monolayer cells and spheroids. (E) cAMP levels of 2D (monolayer cells) versus 3D (spheroids) in naive and chemo-treated cells. (F) Cell viability assay of MDA-MB-231 mammospheres after Rlm treatment for 24 h. (G) Expression of PDE4A1 in MDA-MB-231 mammospheres without and with 10 mM Rlm treatment. (H) cAMP levels of 5 and 10 mM Rlm-treated MDA-MB-231 mammospheres as compared to untreated control. (I) Expression of SOX2, OCT4, NANOG, ABCG2, and ALDH1A1 in mammospheres upon treatment with Rlm (10 mM) as compared to untreated controls. Values indicate fold changes in protein expression corresponding to band intensity. Molecular weights are indicated in kilodalton (kDa). Data are presented as mean \pm SD and are representative of three independent experiments. ALDH, aldehyde dehydrogenase; cAMP, cyclic adenosine 3', 5' monophosphate; MTT, 3-(4,4-dimethylthiazol-2-yl)-2,5 diphenyltetrazolium bromide; PDE4A, phosphodiesterase 4A; Rlm, rolipram. * $p < 0.05$; ** $p < 0.01$; *** $p < 0.001$.

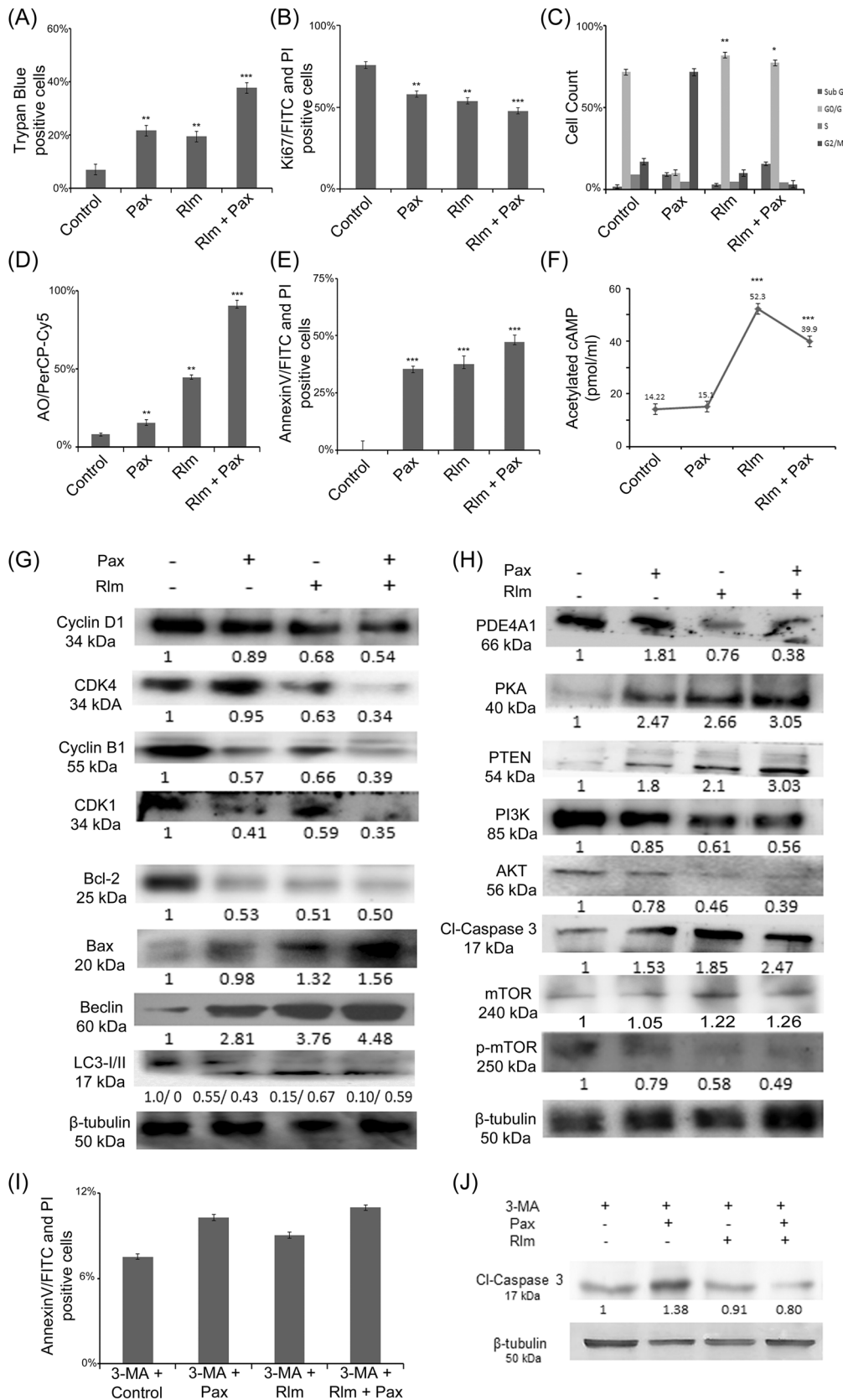


FIGURE 3 (See caption on next page)

and Supporting Information: Figure S2E. That cell death was a result of autophagy (Supporting Information: Figure S2F) and induced apoptosis was confirmed when MDA-MB-231 cells were pretreated with the autophagy inhibitor 3-MA (2 mM for 3 h), followed by treatment with Rlm, Pax, and Rlm + Pax for 24 h (Figure 3I and Supporting Information: Figure S2F). The results clearly indicated that inhibition of autophagy prevented significant cell death in Rlm + Pax treatments (15.69%) as compared to the untreated control (12.16%). This was further validated by invariant cl-caspase 3 expression in the 3MA + Rlm + Pax-treated cells as compared to the control (3MA-treated only; Figure 3J).

3.4 | Rlm facilitates Pax effectiveness and promotes apoptosis in brCSCs by stabilizing Beclin1/Bcl-2 interaction

Rlm treatment (10 mM; 24 h) of mammospheres reduced ALDH⁺ (>3-fold, $p < 0.001$) and CD44⁺/CD24⁻ cells (>3-fold; $p < 0.01$) in contrast to Pax treatment individually (Figure 4A). In addition, Rlm significantly reduced the expression of major stem cell markers, viz., SOX2, OCT4, ALDH1A1, and ABCG2 in mammospheres, either individually or in combination with Pax (Figure 4B). Since Pax treatment had no significant effect on mammospheres, pretreatment of the spheres with Rlm was carried out for 24 h before Pax treatment. Interestingly, Rlm pretreatment (10 mM) followed by Pax treatment (7 nM; 24 h) completely abrogated the spheroid structures in vitro (Figure 4C), indicating that Rlm pretreatment sensitized the chemoresistant brCSCs to the effects of Pax, by

increasing the chemosensitivity of MDA-MB-231-derived mammospheres from 80 to 40 nM ($p < 0.01$; Figure 4D). Rlm treatment significantly increased sub-G₁ population of mammospheres as compared to control (1.7-fold; $p < 0.001$) and Pax treatment individually (1.9-fold; Figure 4E). However, Rlm treatment contributed to moderate autophagy in mammospheres (16.43%; $p < 0.001$) in contrast to Pax treatment individually (96.23%) as seen by flow cytometry/acridine orange staining (Figure 4F). On the contrary, Rlm induced significant apoptosis in mammospheres (44.3%; $p < 0.001$) compared to Pax treatment alone (22.9%) as seen by annexin V/PI staining (Figure 4G). These observations were further supported by western blot analyses, which showed significant upregulation of Bax and downregulation of Bcl-2, Beclin1, and LC3-II/I ratio in the treated mammospheres (Figure 4H). Coimmunoprecipitation of Beclin1/Bcl-2 after treatment with Rlm confirmed a temporal increase in the Beclin1-bound Bcl-2 expression, which stabilized by 72 h (Figure 4I). Rlm reduces the stemness of mammospheres and renders them more chemosensitive to conventional chemotherapeutic drug Pax. The combination of Rlm + Pax not only enhances the effectivity of Pax in targeting triple-negative brCSCs, but also reduces the cell survival autophagy and leads them to caspase-mediated apoptosis.

3.5 | Rlm targets brCSCs by modulating the cAMP/PKA/mTOR axis

TNBC patient-derived brCSCs revealed a time-dependent increase in intracellular cAMP (15.3–53.7 pmol/ml;

FIGURE 3 Rlm induces cell death in combination with paclitaxel through autophagy-mediated apoptosis in breast cancer cells. (A) Representative bar diagram of trypan blue dye exclusion test of MDA-MB-231 cells treated with Rlm (1 mM), Pax (2 nM), and a combination of Rlm + Pax for 24 h. (B) Representative bar diagram of proliferation assay using FITC-tagged Ki67 in MDA-MB-231 cells treated with Rlm (1 mM), Pax (2 nM), and a combination of Rlm + Pax for 24 h. (C) Representative bar diagram of cell cycle analysis of propidium iodide-stained MDA-MB-231 cells showing cell cycle arrest after 24 h treatment with Rlm (1 mM), Pax (2 nM), and a combination of the two for 24 h. (D) Representative bar diagram of acridine orange positive staining from MDA-MB-231 cells after 24 h treatment with Rlm (1 mM), Pax (2 nM), and a combination for 24 h. (E) Representative bar graph of annexin V FITC/PI staining of MDA-MB-231 cells showing populations corresponding to proliferating (Annexin V⁻ PI⁻), early apoptotic (Annexin V⁺ PI⁻), and late (Annexin V⁺ PI⁺) apoptotic cells treated with Rlm (1 mM), Pax (2 nM), and a combination for 24 h. (F) cAMP levels in MDA-MB-231 cells after 24 h treatment of Rlm (1 mM), Pax (2 nM), and combination doses. (G) Expression of Cyclin D1, CDK4, Cyclin B1, CDK1, Bcl-2, Bax, Beclin1, and LC3-I/II from MDA-MB-231 cells upon treatment with Rlm (1 mM), Pax (2 nM), and combination for 24 h. (H) Expression of PDE4A1, PKA, PTEN, PI3K, AKT, cl-caspase 3, mTOR, and pmTOR in MDA-MB-231 cells after treatment with Rlm (1 mM), Pax (2 nM), and a combination of the two for 24 h. (I) Annexin V FITC/PI staining of MDA-MB-231 cells treated with Rlm (1 mM), Pax (2 nM), and combination doses, pre-incubated with the autophagy inhibitor 3-MA (2 mM for 3 h). (J) Expression of cl-caspase 3 in MDA-MB-231 cells pre-incubated with 3-MA (2 mM), followed by treatment with Rlm (1 mM), Pax (2 nM), and a combination of Rlm + Pax. Values indicate fold changes in protein expression corresponding to band intensity. Molecular weights are indicated in kilodalton (kDa). Data are representative of three independent experiments. cl-caspase 3, Cleaved caspase 3; cAMP, cyclic adenosine 3',5' monophosphate; FITC, fluorescein isothiocyanate; PDE4A, phosphodiesterase 4A; Pax, paclitaxel; PKA, protein kinase A; PI3K, phosphatidylinositol-3-kinase; pmTOR, phospho-mTOR; Rlm, rolipram. * $p < 0.05$; ** $p < 0.01$; *** $p < 0.001$.

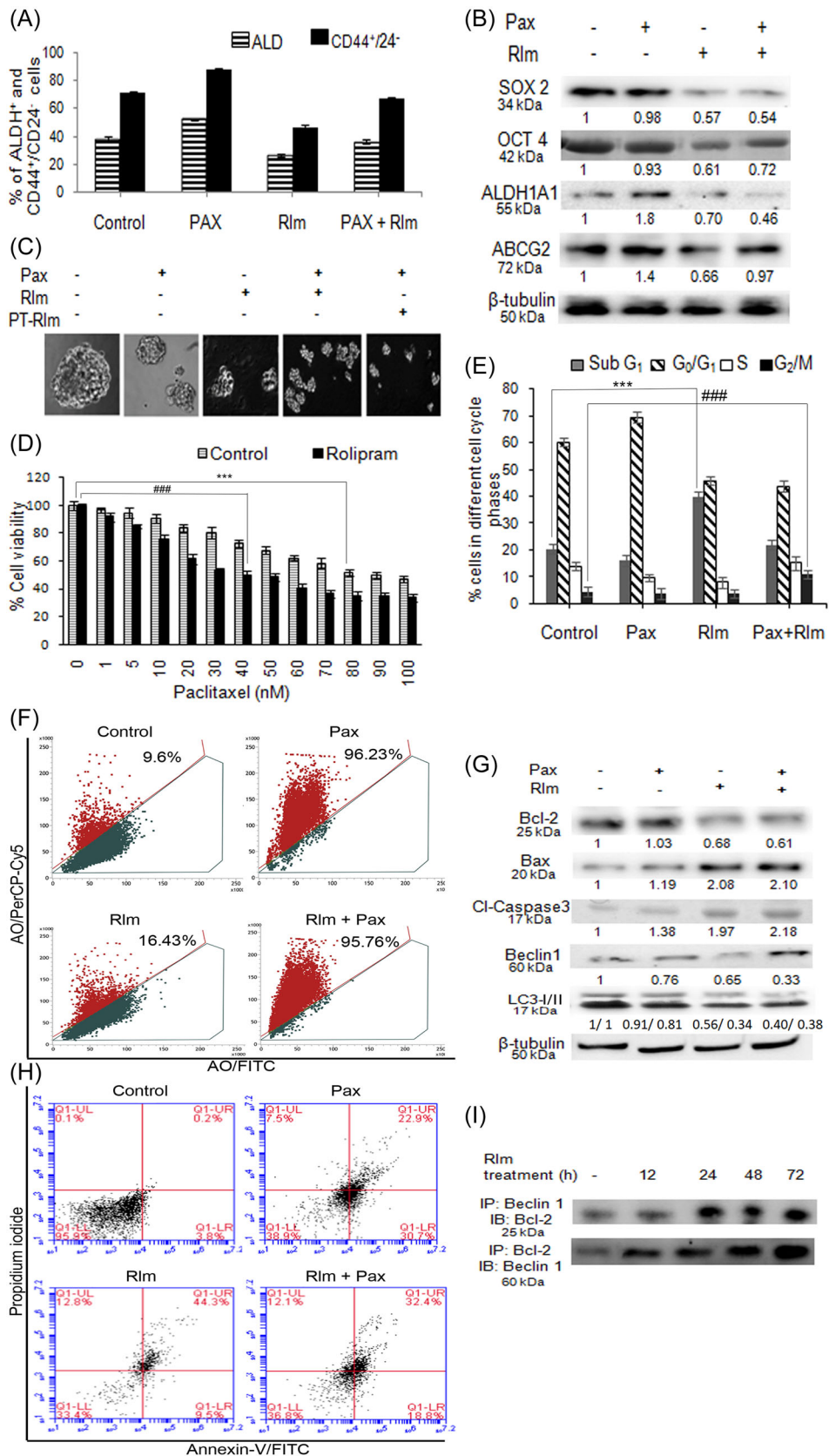


FIGURE 4 (See caption on next page)

$p = 0.000185$) from 12 to 72 h, respectively, when treated with Rlm (10 mM) (Figure 5A), concomitant with significant inhibition of PDE4A1 protein level (Figure 5B). Increased cAMP levels led to a subsequent increase in PKA and PTEN expression, a decrease in PI3K, AKT, and mTOR, and increased pmTOR expression in the TNBC brCSCs (Figure 5B). The pmTOR/mTOR ratio as calculated from the densitometric analyses was observed to be 1 (control), 1.06 (12 h), 2.37 (24 h), 1.51 (48 h), and 1.35 (72 h), indicating maximum pmTOR expression at 24 h (Figure 5B). Subsequently, reduced LC3-I/II expression was observed and the ratio of LC3-I/II was calculated by densitometric analysis (Figure 5C). Trivial changes were seen in Bax and cl-caspase 3 expressions upon Rlm treatment (10 mM) on TNBC brCSCs, but a significant increase in cleaved-PARP expression indicated DNA damage, leading to necrotic death of the spheroids (Figure 5C). Changes in the cell death markers were also reflected in flow cytometric studies, which indicated decreased autophagy in Rlm-treated TNBC brCSCs from 48.7% in control to 10.83% in 72 h ($p < 0.001$; Figure 5D) and increased cell death (Figure 5D). Flow cytometry plots for autophagy and cell death are included in Supporting Information: Figures S3A and S3B, respectively. Results further indicated that silencing of PKA using specific siRNAs or using the PKA-specific inhibitor H89 in TNBC-brCSCs reduced expressions of both PTEN and pmTOR (Figure 5E and Supporting Information: Figure S4A), in response to 10 mM Rlm treatment, authenticating a direct effect of PKA on mTOR in the CSC population. The expressions of mTOR and pmTOR also indicated ratios of pmTOR/mTOR as 1, 1.55, 0.75, and 0.83 in control siRNA, Rlm-treated control siRNA,

PKA-siRNA, and Rlm-treated PKA-siRNA, respectively (Figure 5C). For the docking studies of mTORC-PKAR1 α complex, HADDOCK was implemented, which uses ambiguous interaction restraints to drive the docking. Analysis of the interaction interface and stabilization energy for best-docked structures (Figure 5Fa,b) revealed that both the proteins have considerable patches of interaction area of 1771.3 \AA^2 with ΔG of -10.3 kcal/mol, indicating potential interaction between the two proteins (Figure 5Fc,d). Additionally, coimmunoprecipitation studies using control siRNA, PKA-siRNA, Rlm-treated control siRNA, and Rlm-treated PKA-siRNA reinforced a direct association between PKAR1 α and mTOR (Figure 5G). Coimmunoprecipitation studies were also performed with the H89 treatment of the cells, where a direct association of PKAR1 α and mTOR was observed (Supporting Information: Figure S4B). Silencing of PKA using siRNA and inhibition using H89 in TNBC-derived brCSCs also significantly reduced the expression of stem cell markers SOX2 and ALDH1A1, in response to Rlm treatment (Figure 5H and Supporting Information: Figure S4C). Based on the above findings, an alternate signaling pathway was reconstructed highlighting cAMP-induced PKA as a direct activator of mTOR in brCSCs following exposure to Rlm, which eventually led to abrogation of autophagy and induction of cell death (Figure 5I). Rlm can therefore be a novel candidate in targeting triple-negative brCSCs, which have received prior chemotherapy. Rlm specifically targeted PDE4A1 and enhanced PKA_{active} components by modulating cAMP levels. The PKA_{active} can act as a dual regulator, stimulating mTOR and reducing cell survival autophagy on one hand and enhancing PTEN/PI3K/Akt-mediated apoptosis on the other. These simultaneous effects

FIGURE 4 Rolipram augments paclitaxel effectiveness inducing the death of brCSCs by stabilizing Beclin1/Bcl-2 interaction. (A) Aldefluor assay and CD44/24 analysis of brCSCs treated with Rlm (10 mM), Pax (7 nM), and a combination of Rlm + Pax for 24 h indicates the effectiveness of Rlm compared to the combination dose. (B) Expression of SOX2, OCT4, ALDH1A1, and ABCG2 in mammospheres after treatment with Rlm (10 mM), Pax (7 nM), and a combination for 24 h. (C) Fate of mammospheres after treatment with Pax (7 nM), Rlm (10 mM), and pretreatment with Rlm (PT + Rlm) for 24 h, followed by Pax treatment ($\times 20$ magnification). (D) Pax-chemosensitivity assay of MDA-MB-231 mammospheres pretreated with Rlm (10 mM) for 24 h. #### denotes reduction of sensitivity from 80 to 40 nM when spheres were pretreated with Rlm. (E) Cell cycle analysis of MDA-MB-231 mammospheres treated with Rlm (10 mM), Pax (7 nM), and combination for 24 h. *** denotes an increase in sub-G₁ cells; #### denotes the G₂/M phase arrest. (F) Acridine orange staining and detection of red and green fluorescence of MDA-MB-231 mammospheres after 24 h treatment with Rlm (10 mM), Pax (7 nM), and a combination. (G) Annexin V FITC/PI staining of MDA-MB-231 mammospheres showing populations corresponding to proliferating (Annexin V⁻/PI⁻), early (Annexin V⁺/PI⁻), and late (Annexin V⁺/PI⁺) apoptotic cells treated with Rlm (10 mM), Pax (7 nM), and a combination for 24 h. (H) Expression of Bcl-2, Bax, cl-caspase 3, Beclin1, and LC3-I/II from MDA-MB-231 mammospheres upon treatment with Rlm (10 mM), Pax (7 nM), and a combination for 24 h. Values indicate fold changes in protein expression corresponding to band intensity. Molecular weights are indicated in kilodalton (kDa). (I) Coimmunoprecipitation of Beclin1 and Bcl-2 in Rlm-treated (10 mM) mammosphere extracts at different time points (12, 24, 48, and 72 h) shows the association between autophagy and antiapoptotic markers. Data are presented as mean \pm SD and are representative of three independent experiments. ALDH, aldehyde dehydrogenase; brCSC, breast CSC; cl-caspase 3, cleaved caspase 3; FITC, fluorescein isothiocyanate; Pax, paclitaxel; Rlm, rolipram. #### $p < 0.001$; *** $p < 0.001$.

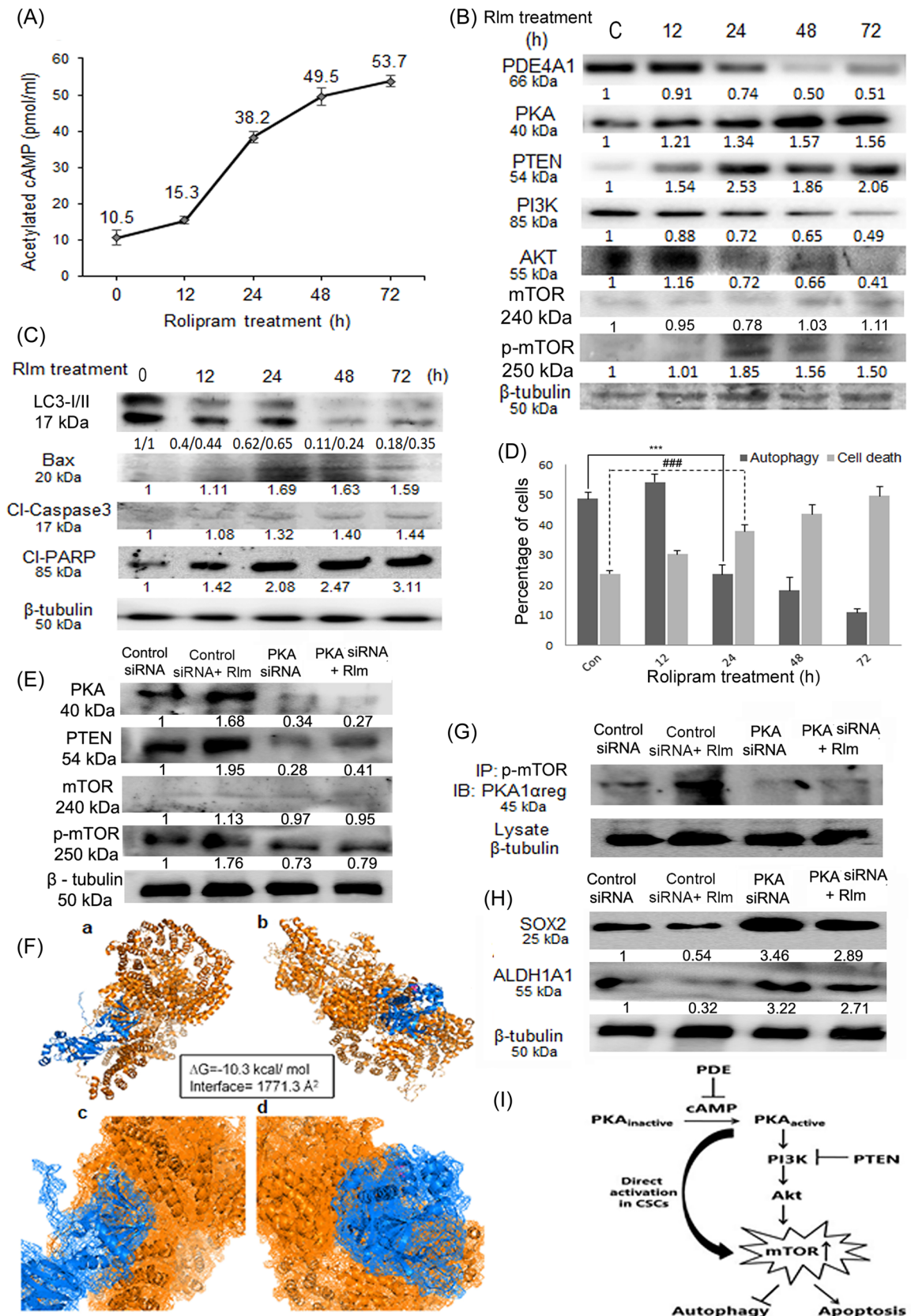


FIGURE 5 (See caption on next page)

ultimately led to the abrogation of spheres, as indicated by reduced expression of the major stem cell markers that play important role in brCSC maintenance.

4 | DISCUSSION

Relapse and metastasis remain major obstacles in the improvement of overall cancer survival and are implicated in the small subpopulation of CSCs, which remain invincible even after surgery, radiotherapy, and chemotherapy. Hence, a successful and sustainable remedy requires the identification of drugs targeting CSCs individually or combining anti-CSC drugs with conventional therapies. PI3Ks are a family of lipid kinases that play an important role in regulating various physiological functions and cellular processes.⁴³ Deregulation of the PI3K signaling pathway has been implicated in a wide range of tumor types.⁴⁴ Therefore, upregulation of PI3K expression in brCSCs, as evident from a differential gene expression analysis,² warranted further investigation to meet the rising need for effective compounds that would abrogate CSCs and cater to successful therapeutic regimes for cancer treatment.

To date, the cellular mechanisms that regulate the sustenance of CSCs are poorly understood, although accumulating evidence has shown that PI3K/Akt/mTOR signaling pathway plays a critical role in the maintenance of CSCs.⁴⁵ In breast cancer, mTOR activation is required for continuance and viability of CSCs, and activation of PI3K/Akt, achieved by knocking down PTEN, is known to enrich breast CSCs.⁴⁶ In prostate cancer cells, stable knockdown of PTEN by short hairpin RNA resulted in an increased sphere-forming ability as

well as increased clonogenic and tumorigenic potential. Meanwhile, inhibition of the PI3K pathway by specific inhibitors reduced stem-like populations in prostate cancer cell lines (64). These reports strongly imply that the PI3K/mTOR pathway is critical for the maintenance of CSCs and that targeting PI3K signaling may be prudent in cancer treatment.⁴⁷ So far, direct mTOR and PI3K inhibitors have been used as anticancer drugs in most tumor types, but with limited anticancer efficacy. Hence, compounds that would target additional components of the PI3K signaling pathway could prove to be more practicable as chemo-drugs. Consequently, this study explicated the effect of a PDE inhibitor on differential coordination of the two major regulators of PI3K, viz. PKA and PTEN. Our results vividly indicated that Rlm could stimulate autophagy-induced cell death in TNBC cells by reducing the expression of PDE4, increasing cAMP levels, enhancing the expression of PKA and PTEN, and modulating expressions of PI3K, Akt, and mTOR, eventually leading to apoptosis. That apoptosis was autophagy-induced was confirmed by the fact that blocking autophagy with 3-MA could prevent apoptosis, as evident from annexin V assays and reduced expression of cl-caspase 3.

Notably, Rlm specifically targeted and exhibited profound effects on the CSCs, as demonstrated by warped mammosphere formation and reduced expression of stemness markers. Concomitant with preferential targeting of CSCs compared with Pax, Rlm effectively inhibited the expression of PDE4, raised the levels of cAMP, and enhanced apoptosis by repressing the expression of PI3K in brCSCs. Since the PI3K pathway plays a pivotal role in self-renewal and maintenance of breast CSCs, our results establish that Rlm is more

FIGURE 5 PKA directly alters mTOR expression to regulate the fate of brCSCs. (A) cAMP levels of TNBC mammospheres after treatment of Rlm (10 mM) at different time points. (B) Expression of PDE4A1, PKA, PTEN, PI3K, AKT, mTOR, and pmTOR in TNBC mammospheres after treatment with Rlm (10 mM) at different time points. (C) Expression of LC3-I/II, Bax, cl-caspase 3, and cl-PARP in TNBC mammospheres after treatment of Rlm (10 mM) at different time points. (D) Histograms showing autophagic (acridine orange stained) and dead (Annexin V FITC/PI-stained) cell populations as indicated by flow cytometry from TNBC mammospheres after treatment with Rlm (10 mM) at different time points. (E) Expression of PKA, PTEN, mTOR, and pmTOR in control siRNA-transfected and PKA-specific siRNA-transfected TNBC mammospheres with subsequent Rlm treatment (10 mM, 24 h). (F) The predicted structure of the mTORC–PKAR1 α complex, with mTORC shown in blue and PKAR1 α in orange. Side view (a) and top view (b) of the predicted complex are shown. The interface of the interaction is shown in mesh (c, side view; d, top view). The ΔG and interface area are mentioned in the inset box. (G) Coimmunoprecipitation of mTOR and PKA1 α reg after PKA siRNA transfection and control siRNA transfection with subsequent Rlm (10 mM) treatment for 24 h in TNBC mammosphere extracts showing an association between these regulators at the protein level. (H) Expression of SOX2 and ALDH1A1 in TNBC mammospheres treated with Rlm (10 μ M) after transfection using control siRNA and PKA siRNA. Values indicate fold changes in protein expression corresponding to band intensity. Molecular weights are indicated in kilodalton (kDa). Data are presented as mean \pm SD and are representative of three independent experiments. $###p < 0.001$; $***p < 0.001$. (I) Schematic representation of the mode of action of Rlm in brCSCs. ALDH, aldehyde dehydrogenase; brCSC, breast CSC; cAMP, cyclic adenosine 3', 5' monophosphate; pmTOR, phospho-mTOR; PDE4A, phosphodiesterase 4A; PI3K, phosphatidylinositol-3-kinase; PKA, protein kinase A; PTEN, phosphatase and tensin homolog; Rlm, rolipram; siRNA, small interfering RNA; TNBC, triple-negative breast tumor.

effective in targeting the PI3K/Akt/mTOR pathway than Pax. Often, it has been observed that targeting only the putative rare CSC population in advanced solid tumors may have little effect on patient prognosis.⁴⁸ Hence, combining traditional chemotherapies with novel CSC-targeting agents assures to be an efficient therapeutic strategy. As reported, Pax, a chemotherapeutic agent commonly used to treat breast cancer, enriched CSCs in breast tumors, thereby enhancing the risk of disease recurrence.² However, in the presence of Rlm, or more effectively after pretreatment with Rlm, Pax effectively eliminated CSCs. Rlm not only reduced chemoresistance but facilitated the anticancer effects of Pax in mammospheres, indicating a pharmacodynamic interaction with a promise of sustainable synergistic effects. We also observed a temporal occurrence of decreased autophagy and increased apoptosis when mammospheres were treated with Rlm. This defines a survival versus death response to the PDE inhibitor, since at early time points, autophagy prevails with almost no cell death; however, by 24 h autophagy is reduced and cell death ensues, reaching the pinnacle within 72 h.⁴⁹ Interestingly, the proapoptotic effects were in part a result of the stable association between Beclin1 and Bcl-2, which facilitated cell death. Pax is a bioactive diterpene that has been shown to affect various signal transduction pathways. In one of their recent work, Ren et al.⁵⁰ demonstrated that Pax treatment negatively impacts AKT cascade and escalate P38MAPK and p90RS6K. Such pathways can potentially affect the PI3K–mTOR–PKA axis explored here. Additionally, the differential impact of Pax and Rlm on apoptotic and autophagy pathways warrants future introspection of their influence on apoptosis–autophagy crosstalk nodes like Bcl-2/Beclin1, caspase 3/6, p53-DRAM, and FLIP.

An interesting paradox emerged from this study. Contrary to that seen in the breast cancer cells where Rlm treatment reduced mTOR expression, treatment of breast CSCs with Rlm led to an increased expression of mTOR. Elucidating upstream components revealed a direct influence of PKA on mTOR, bypassing the canonical pathway components, viz. PI3K and Akt, since inhibition of PKA with both the chemical inhibitor H89- and PKA-specific siRNA modulated the expression of pmTOR. This not only led to time-dependent decrease in autophagy but promoted obliteration of the brCSCs, as evident from increased PARP cleavage. That reduction of autophagy in the mammospheres is an outcome of increased mTOR expression has led us to deviate from the putative signaling pathway confirmed in breast cancer cells and consider direct activation of mTOR by PKA in the breast CSC population. Our speculation was further substantiated by docking studies, which predicted

strong interactions between mTOR and PKAR1 α . Additionally, coimmunoprecipitation studies further authenticated this conjecture. Concomitantly, increased PKA resulted in the gain of PTEN function, which also contributed to cell death. Therefore, in an attempt to counteract signaling components, which help maintain stemness properties of CSCs, a noncanonical activation of mTOR by Rlm was identified, which led to selective elimination of the CSCs. This finally achieved the objective of obliterating CSCs, and assured reducing the risk of tumor recurrence in patients. Overall, in contrast to the conventionally used chemo-drug Pax, Rlm was more effective in specifically targeting the CSCs and could therefore be developed as an anticancer drug to be used individually or in combination with other conventional drugs in future for sustained therapeutic benefits and better patient prognosis.

AUTHOR CONTRIBUTIONS

Pritha Mukherjee, Arka Bagchi, and Ananya Banerjee performed the experiments, helped in the analysis and interpretation of data, and drafted the manuscript. Arijit Bhattacharya contributed to the docking studies. Himansu Roy contributed to the procurement and validation of human normal breast and tumor samples. Arunima Biswas and Urmi Chatterji contributed to the conception and design of the study, data interpretation, and finalizing the manuscript. All the authors approved the final version of the manuscript.

ACKNOWLEDGMENTS

The authors thank the Department of Biotechnology, Government of West Bengal, India [No. 248 (Sanc)/BT (Estt)/RD-27/2016] for funding this study and would like to acknowledge the DST-PURSE-sponsored instrument facilities of the Universities of Kolkata and Kalyani. The authors would also like to thank the DST-FIST and UGC-SAP programmes of the Department of Zoology, University of Calcutta and University of Kalyani for providing instrument and infrastructure facilities. The authors acknowledge the help from the Personal Research Grant, University of Kalyani. We are also thankful to the BD-CoE, Centre for Research in Nanoscience and Nanotechnology, University of Calcutta and Dr. Ritesh Tiwari for help with flow cytometry.

CONFLICT OF INTEREST

The authors declare no conflict of interest.

DATA AVAILABILITY STATEMENT

The data that support the findings of this study are available from the corresponding author upon reasonable request.

ORCID

Urmi Chatterji  <http://orcid.org/0000-0002-9317-5672>

REFERENCES

- Das S, Mukherjee P, Chatterjee R, Jamal Z, Chatterji U. Enhancing chemosensitivity of breast cancer stem cells by downregulating SOX2 and ABCG2 using wedelolactone-encapsulated nanoparticles. *Mol Cancer Ther.* 2019;18(3):680-692. doi:10.1158/1535-7163.MCT-18-0409
- Mukherjee P, Gupta A, Chattopadhyay D, Chatterji U. Modulation of SOX2 expression delineates an end-point for paclitaxel-effectiveness in breast cancer stem cells. *Sci Rep.* 2017;7(1):9170. doi:10.1038/s41598-017-08971-2
- Xia P, Xu XY. PI3K/Akt/mTOR signaling pathway in cancer stem cells: from basic research to clinical application. *Am J Cancer Res.* 2015;5(5):1602-1609.
- Chen S, Fisher RC, Signs S, et al. Inhibition of PI3K/Akt/mTOR signaling in PI3KR2-overexpressing colon cancer stem cells reduces tumor growth due to apoptosis. *Oncotarget.* 2016;8(31):50476-50488. doi:10.18632/oncotarget.9919
- Honjo S, Ajani JA, Scott AW, et al. Metformin sensitizes chemotherapy by targeting cancer stem cells and the mTOR pathway in esophageal cancer. *Int J Oncol.* 2014;45(2):567-574. doi:10.3892/ijo.2014.2450
- Li H, Zeng J, Shen K. PI3K/AKT/mTOR signaling pathway as a therapeutic target for ovarian cancer. *Arch Gynecol Obstet.* 2014;290(6):1067-1078. doi:10.1007/s00404-014-3377-3
- Mohammed A, Janakiram NB, Brewer M, et al. Antidiabetic drug metformin prevents progression of pancreatic cancer by targeting in part cancer stem cells and mTOR signaling. *Transl Oncol.* 2013;6(6):649-659. doi:10.1593/tlo.13556
- Tapia O, Riquelme I, Leal P, et al. The PI3K/AKT/mTOR pathway is activated in gastric cancer with potential prognostic and predictive significance. *Virchows Archiv.* 2014;465(1):25-33. doi:10.1007/s00428-014-1588-4
- Bellacosa A, De Feo D, Godwin AK, et al. Molecular alterations of the AKT2 oncogene in ovarian and breast carcinomas. *Int J Cancer.* 1995;64(4):280-285. doi:10.1002/ijc.2910640412
- Cheng JQ, Ruggeri B, Klein WM, et al. Amplification of AKT2 in human pancreatic cells and inhibition of AKT2 expression and tumorigenicity by antisense RNA. *Proc Natl Acad Sci USA.* 1996;93(8):3636-3641. doi:10.1073/pnas.93.8.3636
- Porta C, Paglino C, Mosca A. Targeting PI3K/Akt/mTOR signaling in cancer. *Front Oncol.* 2014;4:64. doi:10.3389/fonc.2014.00064
- Cosentino C, Di Domenico M, Porcellini A, et al. p85 regulatory subunit of PI3K mediates cAMP-PKA and estrogens biological effects on growth and survival. *Oncogene.* 2007;26(14):2095-2103. doi:10.1038/sj.onc.1210027
- Ariga M, Nedachi T, Akahori M, et al. Signalling pathways of insulin-like growth factor-I that are augmented by cAMP in FRTL-5 cells. *Biochem J.* 2000;348(pt 2):409-416.
- Pastan IH, Johnson GS, Anderson WB. Role of cyclic nucleotides in growth control. *Annu Rev Biochem.* 1975;44:491-522. doi:10.1146/annurev.bi.44.070175.002423
- Dumaz N, Light Y, Marais R. Cyclic AMP blocks cell growth through Raf-1-dependent and Raf-1-independent mechanisms. *Mol Cell Biol.* 2002;22(11):3717-3728. doi:10.1128/MCB.22.11.3717-3728.2002
- Magnaldo I, Pouysségur J, Paris S. Cyclic AMP inhibits mitogen-induced DNA synthesis in hamster fibroblasts, regardless of the signalling pathway involved. *FEBS Lett.* 1989;245(1-2):65-69. doi:10.1016/0014-5793(89)80193-0
- Gerits N, Kostenko S, Shiryaev A, Johannessen M, Moens U. Relations between the mitogen-activated protein kinase and the cAMP-dependent protein kinase pathways: comradeship and hostility. *Cell Signal.* 2008;20(9):1592-1607. doi:10.1016/j.cellsig.2008.02.022
- Sassone-Corsi P. The cyclic AMP pathway. *Cold Spring Harbor Perspect Biol.* 2012;4(12):a011148. doi:10.1101/cshperspect.a011148
- Fajardo AM, Piazza GA, Tinsley HN. The role of cyclic nucleotide signaling pathways in cancer: targets for prevention and treatment. *Cancers.* 2014;6(1):436-458. doi:10.3390/cancers6010436
- Sodani K, Patel A, Kathawala RJ, Chen ZS. Multidrug resistance associated proteins in multidrug resistance. *Chin J Cancer.* 2012;31(2):58-72. doi:10.5732/cjc.011.10329
- Cheepala S, Hulot JS, Morgan JA, et al. Cyclic nucleotide compartmentalization: contributions of phosphodiesterases and ATP-binding cassette transporters. *Annu Rev Pharmacol Toxicol.* 2013;53:231-253. doi:10.1146/annurev-pharmtox-010611-134609
- Wielinga PR, van der Heijden I, Reid G, Beijnen JH, Wijnholds J, Borst P. Characterization of the MRP4- and MRP5-mediated transport of cyclic nucleotides from intact cells. *J Biol Chem.* 2003;278(20):17664-17671. doi:10.1074/jbc.M212723200
- Beavo JA, Brunton LL. Cyclic nucleotide research—still expanding after half a century. *Nat Rev Mol Cell Biol.* 2002;3(9):710-718. doi:10.1038/nrm911
- Ahn YH, Jung JM, Hong SH. 8-Chloro-cyclic AMP-induced growth inhibition and apoptosis is mediated by p38 mitogen-activated protein kinase activation in HL60 cells. *Cancer Res.* 2005;65(11):4896-4901. doi:10.1158/0008-5472.CAN-04-3122
- Jiang X, Li J, Paskind M, Epstein PM. Inhibition of calmodulin-dependent phosphodiesterase induces apoptosis in human leukemic cells. *Proc Natl Acad Sci USA.* 1996;93(20):11236-11241. doi:10.1073/pnas.93.20.11236
- Zhu B, Strada SJ. The novel functions of cGMP-specific phosphodiesterase 5 and its inhibitors in carcinoma cells and pulmonary/cardiovascular vessels. *Curr Top Med Chem.* 2007;7(4):437-454. doi:10.2174/156802607779941198
- Johansson CC, Yndestad A, Enserink JM, Ree AH, Aukrust P, Taskén K. The epidermal growth factor-like growth factor amphiregulin is strongly induced by the adenosine 3', 5'-monophosphate pathway in various cell types. *Endocrinology.* 2004;145(11):5177-5184. doi:10.1210/en.2004-0232
- Marko D, Pahlke G, Merz KH, Eisenbrand G. Cyclic 3', 5'-nucleotide phosphodiesterases: potential targets for anticancer therapy. *Chem Res Toxicol.* 2000;13(10):944-948. doi:10.1021/tx000090l
- Bloom HJ, Richardson WW. Histological grading and prognosis in breast cancer; a study of 1409 cases of which 359 have been followed for 15 years. *Br J Cancer.* 1957;11(3):359-377. doi:10.1038/bjc.1957.43

30. Mahajan SD, Law WC, Aalinkeel R, et al. Nanoparticle-mediated targeted delivery of antiretrovirals to the brain. *Methods Enzymol.* 2012;509:41-60. doi:10.1016/B978-0-12-391858-1.00003-4
31. Al-Wadei HA, Takahashi T, Schuller HM. Growth stimulation of human pulmonary adenocarcinoma cells and small airway epithelial cells by β -carotene via activation of cAMP, PKA, CREB and ERK1/2. *Int J Cancer.* 2006;118(6):1370-1380. doi:10.1002/ijc.21537
32. Cummings BS, Schnellmann RG. Measurement of cell death in mammalian cells. *Curr Protoc Pharmacol.* 2004;12. doi:10.1002/0471141755.ph1208s25
33. Filippi-Chiela EC, Villodre ES, Zamin LL, Lenz G. Autophagy interplay with apoptosis and cell cycle regulation in the growth inhibiting effect of resveratrol in glioma cells. *PLoS One.* 2011;6(6):e20849. doi:10.1371/journal.pone.0020849
34. Pattingre S, Tassa A, Qu X, et al. Bcl-2 antiapoptotic proteins inhibit Beclin 1-dependent autophagy. *Cell.* 2005;122(6):927-939. doi:10.1016/j.cell.2005.07.002
35. Kiefer F, Arnold K, Künzli M, Bordoli L, Schwede T. The SWISS-MODEL Repository and associated resources. *Nucleic Acids Res.* 2009;37:D387-D392. doi:10.1093/nar/gkn750
36. Benkert P, Biasini M, Schwede T. Toward the estimation of the absolute quality of individual protein structure models. *Bioinformatics.* 2011;27(3):343-350.
37. Laskowski RA, Rullmann JA, MacArthur MW, Kaptein R, Thornton JM. AQUA and PROCHECK-NMR: programs for checking the quality of protein structures solved by NMR. *J Biomol NMR.* 1996;8(4):477-486. doi:10.1007/BF00228148
38. Peters B, Moad C, Youn E, Buffington K, Heiland R, Mooney S. Identification of similar regions of protein structures using integrated sequence and structure analysis tools. *BMC Struct Biol.* 2006;6:4. doi:10.1186/1472-6807-6-4
39. Van Zundert G, Rodrigues J, Trellet M, et al. The HADDOCK2.2 Web Server: user-friendly integrative modeling of biomolecular complexes. *J Mol Biol.* 2016;428(4):720-725. doi:10.1016/j.jmb.2015.09.014
40. De Vries SJ, Bonvin AM. CPORT: a consensus interface predictor and its performance in prediction-driven docking with HADDOCK. *PLoS One.* 2011;6(3):e17695. doi:10.1371/journal.pone.0017695
41. Paxman JJ, Heras B. Bioinformatics tools and resources for analyzing protein structures. *Methods Mol Biol.* 2017;1549:209-220. doi:10.1007/978-1-4939-6740-7_16
42. Xue LC, Rodrigues JP, Kastriitis PL, Bonvin AM, Vangone A. PRODIGY: a web server for predicting the binding affinity of protein-protein complexes. *Bioinformatics.* 2016;32(23):3676-3678. doi:10.1093/bioinformatics/btw514
43. Thorpe LM, Yuzugullu H, Zhao JJ. PI3K in cancer: divergent roles of isoforms, modes of activation and therapeutic targeting. *Nat Rev Cancer.* 2015;15(1):7-24. doi:10.1038/nrc3860
44. Samuels Y, Wang Z, Bardelli A, et al. High frequency of mutations of the PIK3CA gene in human cancers. *Science.* 2004;304(5670):554. doi:10.1126/science.1096502
45. Dubrovskaya A, Kim S, Salamone RJ, et al. The role of PTEN/Akt/PI3K signaling in the maintenance and viability of prostate cancer stem-like cell populations. *Proc Natl Acad Sci USA.* 2009;106(1):268-273. doi:10.1073/pnas.0810956106
46. Zhou J, Wulfschlegel J, Zhang H, et al. Activation of the PTEN/mTOR/STAT3 pathway in breast cancer stem-like cells is required for viability and maintenance. *Proc Natl Acad Sci USA.* 2007;104(41):16158-16163. doi:10.1073/pnas.0702596104
47. Li X, Zhou N, Wang J, et al. Quercetin suppresses breast cancer stem cells (CD44⁺/CD24⁻) by inhibiting the PI3K/Akt/mTOR-signaling pathway. *Life Sci.* 2018;196:56-62. doi:10.1016/j.lfs.2018.01.014
48. Rahman M, Deleyrolle L, Vedam-Mai V, Azari H, Abd-El-Barr M, Reynolds BA. The cancer stem cell hypothesis: failures and pitfalls. *Neurosurgery.* 2011;68(2):531-545. doi:10.1227/NEU.0b013e3181ff9eb5
49. Houslay MD, Kolch W. Cell-type specific integration of cross-talk between extracellular signal-regulated kinase and cAMP signaling. *Mol Pharmacol.* 2000;58(4):659-668. doi:10.1124/mol.58.4.659
50. Ren X, Zhao B, Chang H, Xiao M, Wu Y, Liu Y. Paclitaxel suppresses proliferation and induces apoptosis through regulation of ROS and the AKT/MAPK signaling pathway in canine mammary gland tumor cells. *Mol Med Rep.* 2018;17(6):8289-8299. doi:10.3892/mmr.2018.8868

SUPPORTING INFORMATION

Additional supporting information can be found online in the Supporting Information section at the end of this article.

How to cite this article: Mukherjee P, Bagchi A, Banerjee A, et al. PDE4 inhibitor eliminates breast cancer stem cells via noncanonical activation of mTOR. *J Cell Biochem.* 2022;1-17. doi:10.1002/jcb.30325